

Apodized photonic crystals: A non-dissipative system hosting multiple exceptional points

Abhishek Mondal, Shailja Sharma and Ritwick Das*

*School of Physical Sciences, National Institute of Science Education and Research,
An OCC of Homi Bhabha National Institute, Jatni - 752050, Odisha, India*

(Dated: January 11, 2023)

Optical systems obeying non-Hermitian dynamics have been the subject of intense and concerted investigation over the last two decades owing to their broad implications in photonics, acoustics, electronics as well as atomic physics. A vast majority of such investigations rely on a dissipative, balanced loss-gain system which introduces unavoidable noise and consequently, this limits the coherent control of propagation dynamics. Here, we show that an all-dielectric, non-dissipative photonic crystal (PC) could host, at least two exceptional points in its eigenvalue spectrum. By introducing optimum apodization in the PC architecture, namely 1D-APC, we show that such a configuration supports a spectrum of exceptional points which distinctly demarcates the \mathcal{PT} -symmetric region from the region where \mathcal{PT} -symmetry is broken in the parameter space. The analytical framework allows us to estimate the geometric phase of the reflected beam and derive the constraint that governs the excitation of topologically-protected optical Tamm-plasmon modes in 1D-APCs.

I. INTRODUCTION

Optical systems which are governed by non-Hermitian Hamiltonian dynamics through an engineered gain and dissipation mechanism, provide a route to overcome the limitations imposed by closed optical systems that obey the Hermitian-Hamiltonian led dynamics. Such non-Hermitian systems give rise to a real eigenvalue spectrum when the Hamiltonian commutes with the parity-time (\mathcal{PT}) operator. A continuous change in the parameter governing the Hermiticity (of the Hamiltonian) breaks the \mathcal{PT} symmetry which manifests in the form of complex eigenvalues for the system. In the phase space, such points where the real and complex eigenvalues coalesce are termed as exceptional points (EPs) [1, 2]. This spontaneous \mathcal{PT} -symmetry breaking has catalyzed a plethora of non-intuitive outcomes such as directional invisibility [3, 4], coherent perfect lasing and absorption [5–9], negative refraction [10], single-particle based sensing [11–13], distortion-free wireless optical power transfer [14] and a few more [15–19]. It is, however, worth noting that the incommensurate gain and loss distribution in non-Hermitian systems impose the primary limitation on the practical applications due to unpredictable signal-to-noise ratio near EP [20–23]. In order to circumvent such bottlenecks, a few possibilities have been explored. One such promising route is to create an asymmetric loss in the system (without gain) whose dynamics could be explored using a non-Hermitian Hamiltonian with a uniform background loss [20, 24, 25]. Such a configuration would exhibit \mathcal{PT} -symmetry which could be broken through scaling up the loss asymmetry. In a different scheme, a pseudo-Hermitian system was explored which allowed strong coupling between a large number

of modes via manipulation of the parameters governing the Hamiltonian [24]. This led to the existence of EPs of multiple order and the interaction of eigenvalues around each EP provides a robust control on the propagation dynamics [26, 27]. In spite of the aforementioned developments, a useful and practical proposition would be to devise a configuration hosting a multitude of EPs with the constraint that the electromagnetic (EM) energy lost due to the non-Hermitian dynamics is stored in a reservoir. This essentially implies that the dissipative channel associated with a non-Hermitian system drives a separate Hermitian system which could allow reverse flow of EM energy by virtue of cyclical dynamics. Such systems have been explored in the area of parametric frequency conversion processes where the EM energy lost in one of the parametric processes (obeying non-Hermitian dynamics) is coherently added to the other parametric process that follows a Hermitian dynamics [28]. A plausible translation of such an idea in the non-absorptive linear systems would be to introduce a *virtual* loss in an intermodal interaction process thereby generating multiple EPs in the parameter space. One of the simplest configurations imitating such a process is a multimodal interaction in an all-dielectric one-dimensional (1D) photonic-crystal (PC) with a gradually varying duty cycle (for each unit cell). In such an apodized 1D-PC, the forward (source) to backward (sink) mode-coupling dynamics is essentially governed by a pseudo-Hermitian Hamiltonian whose Hermiticity is determined by the apodization along the propagation direction. In the present work, we show the existence of multiple EPs in an apodized 1D-PC and develop an analytical framework for ascertaining the possibility of exciting topologically-protected optical edge modes in such aperiodically stratified configurations.

* ritwick.das@niser.ac.in

II. THEORETICAL FRAMEWORK AND COUPLED-MODE FORMALISM

We consider a 1D-PC comprised of periodic bilayers with refractive indices n_1 and n_2 with thicknesses d_1 and d_2 . Such conventional 1D-PCs or alternatively, distributed Bragg reflectors (DBRs) are usually characterized by photonic bandgaps (PBGs) which are separated from each other by high transmission (or pass) bands. In order to appreciate the EM wave propagation dynamics, we consider the coupling between p^{th} -mode ($|p\rangle$) with q^{th} -mode ($|q\rangle$) which could be represented employing the coupled-amplitude equations given by [29]

$$\frac{dA_q}{dz} = -i \frac{\beta_q}{|\beta_q|} \sum_p \sum_m \tilde{\kappa}_{qp}^{(m)} A_p e^{-i(\beta_q - \beta_p - m \frac{2\pi}{\Lambda})z} \quad (1)$$

where β_p and β_q are the longitudinal (z) components of wavevector k_p and k_q respectively. $\tilde{\kappa}_{qp}^{(m)}$ defines the strength of coupling (or coupling coefficient) between the p^{th} and q^{th} mode that is coupled through the m^{th} Fourier component of the periodic dielectric distribution ($\Lambda = d_1 + d_2$). The factor $\Delta\beta = \beta_q - \beta_p - m \frac{2\pi}{\Lambda}$ (known as the phase-mismatch) is one of the dynamical variables (along with κ_{qp}) which dictate the measure of optical power transferred from one mode to the other. For the present work, we consider a contra-directional coupling set-up where a forward (along $+z$) propagating mode ($|p\rangle \equiv |f\rangle$) is coupled to a backward (along $-z$) propagating mode ($|q\rangle \equiv |b\rangle$). Accordingly, it could be asserted that $\beta_b = -\beta_f$ or alternatively $\Delta\beta = 2\beta_f - \frac{2\pi}{\Lambda}$ and therefore, Eq. (1) could be simplified to [29]

$$\frac{dA_b}{dz} = i\tilde{\kappa} A_f e^{-i\Delta\beta z} \quad (2)$$

$$\frac{dA_f}{dz} = -i\tilde{\kappa}^* A_b e^{i\Delta\beta z} \quad (3)$$

where $\tilde{\kappa} = \frac{i(1 - \cos 2\pi\zeta)}{2\Lambda} \frac{(n_1^2 - n_2^2)}{\bar{n}} = i\kappa$ and ζ is the dielectric filling fraction of layer with refractive index n_1 in the unit cell *i.e.* $\frac{d_1}{\Lambda}$. The mean refractive index for an unit cell of thickness Λ is $\bar{n} = \sqrt{\frac{d_1 n_1^2 + d_2 n_2^2}{\Lambda}}$. By using a Gauge transformation given by $[A_f, A_b] \rightarrow [\tilde{A}_f, \tilde{A}_b] e^{i/2[\Delta\beta_0 z - \int_0^z q(z') dz']}$, we obtain [30]

$$i \frac{d}{dz} \begin{pmatrix} \tilde{A}_b \\ \tilde{A}_f \end{pmatrix} = \begin{pmatrix} -\Delta k & -\tilde{\kappa} \\ \tilde{\kappa}^* & \Delta k \end{pmatrix} \begin{pmatrix} \tilde{A}_b \\ \tilde{A}_f \end{pmatrix} \quad (4)$$

Equation (4) is analogous to time-dependent Schrödinger's equation with t -coordinate being replaced by z -coordinate. Here, $\Delta k (= \frac{\Delta\beta}{2})$ and $q(z) = 0$ remains constant (for a given frequency) across the 1D-PC which has a fixed duty cycle. The autonomous Hamiltonian $\hat{H} = -\vec{\sigma} \cdot \vec{B}$ with $\vec{\sigma} \equiv [\sigma_x, \sigma_y, \sigma_z]$ are the Pauli's spin matrices and $\vec{B} \equiv [0, \kappa, \Delta k]$ (magnetic field analog) represents a pseudo-Hermitian evolution dynamics. In order

to appreciate this point, we note that the eigenvalues of \hat{H} which are given by $e_{1,2} = \pm \sqrt{\Delta k^2 - \kappa^2}$ whereas the eigenfunctions are $|\psi_1\rangle = \begin{pmatrix} -i \frac{(\Delta k + \sqrt{\Delta k^2 - \kappa^2})}{1} \\ \kappa \end{pmatrix}$ and $|\psi_2\rangle = \begin{pmatrix} +i \frac{(-\Delta k + \sqrt{\Delta k^2 - \kappa^2})}{1} \\ \kappa \end{pmatrix}$. Here, $\tilde{\kappa} = i\kappa$. A

closer look into the eigenvectors reveals that the equality $\kappa = \pm \Delta k$ manifests as coalescing of eigenvectors accompanied by vanishing eigenvalues. Such points in parameter space where κ equals $\pm \Delta k$ are termed as exceptional points (EPs) and they distinctly demarcate the regions exhibiting Hermitian (\mathcal{PT} -symmetric phase) and non-Hermitian (\mathcal{PT} -broken phase) dynamical evolution of states (or modes).

In order to appreciate the aforementioned idea, we consider a practical 1D-PC with $n_1 \equiv TiO_2$ layer and $n_2 \equiv SiO_2$ layer. The layer thicknesses are $d_1 = d_2 = 150 \text{ nm}$. The reflection spectrum for $N = 20$ unit cells is plotted in Fig. 1(a) which exhibits a high reflection band (or PBG) spreading over a 75 THz bandwidth. In order to obtain the reflection spectrum, finite element method (FEM) based simulations were carried out using the commercially available computational tool (COMSOL Multiphysics). In the simulations, the periodic boundary condition is imposed along the transverse direction and a mesh size of 5 nm is considered. We ignore the material dispersion for the simulations and assume $n_1 = 2.5$ ($\equiv TiO_2$) and $n_2 = 1.5$ ($\equiv SiO_2$) across the entire spectrum. For this 1D-PC, we also plotted the eigenvalues e_1 and e_2 (see Fig. 1(b)) as a function of the frequency of the incident electromagnetic wave. It is apparent that the eigenvalues vanish at $\nu_1 \approx 210 \text{ THz}$ and $\nu_2 \approx 285 \text{ THz}$. These two frequencies (ν_1 and ν_2) define the EPs ($\kappa = +\Delta k$ and $\kappa = -\Delta k$) for the periodic 1D-PC. A closer look would also reveal that the eigenvalues are purely imaginary within the PBG and the band edges (Fig. 1 (a)) coincide with ν_1 and ν_2 . The mode fields for frequencies lying inside the PBG (240 THz) and outside the PBG (310 THz) are presented in Figs. 1(c) and (d) respectively. It is worth noting that the investigations on systems exhibiting \mathcal{PT} -symmetry (or \mathcal{PT} -broken symmetry) led dynamics in photonics essentially involve optimally balanced gain-loss architectures such as segmented waveguides and photonic crystals. In such systems, a complex relative permittivity in different sections depicting *actual* gain or loss for the propagating light beam gives rise to the \mathcal{PT} -symmetry (or \mathcal{PT} -broken symmetry). The present configuration involving 1D-PC does not include an *actual* dissipative component for achieving the \mathcal{PT} -symmetric to \mathcal{PT} -symmetry broken phase transition. Alternatively, the coupling of optical power to the backscattered mode $|b\rangle$ is analogous to a *virtual* loss for a forward propagating $|f\rangle$ mode. When this coupling is relatively weak *i.e.* $\Delta k > \tilde{\kappa}$, $|f\rangle$ and $|b\rangle$ exhibits cyclic exchange of optical power (as a function of z) which is a primitive outcome for a \mathcal{PT} -symmetric dynamics. On the other hand, a strong coupling regime

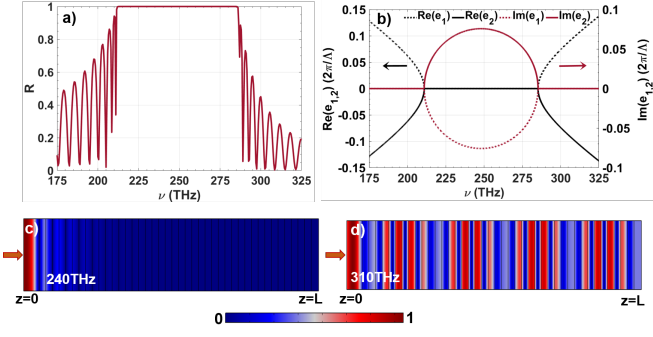


FIG. 1. a) Shows the reflection spectrum of a conventional (periodic) 1D-PC. b) Shows the variation in $Re(e_1)$ (dotted black curve), $Im(e_1)$ (dotted maroon curve), $Re(e_2)$ (solid black curve) and $Im(e_2)$ (solid maroon curve) as a function of frequency (ν). c) and d) Shows the mode-field intensity for frequencies within the PBG 240 THz and that outside the PBG 310 THz respectively. The solid red arrow represents the direction of incidence of light.

where $\Delta k < \tilde{\kappa}$ manifests through a monotonic growth of backscattered mode ($|b\rangle$) that is a signature of \mathcal{PT} -symmetry broken phase. It is worthwhile to reiterate the point that the two regimes depicted by the inequality of Δk and $\tilde{\kappa}$ (in the parameter space) could be mapped onto the PBG and pass or transmission band (s) in the reflected spectrum. Subsequently, each PBG is necessarily bounded by two EPs in this framework. Additionally, these two EPs are fixed and could not be tailored for a given 1D-PC with a fixed duty cycle and fixed period. Also, the conventional 1D-PC geometry excludes the possibility of realizing higher-order exceptional points [31]. Taking a cue from this critical viewpoint, we note that a small apodization or gradual change in dielectric filling fraction (ζ) of each unit cell of the 1D-PC would allow us to realize discretely spaced (multiple) EPs at different optical frequencies (or wavelengths). In order to elucidate this point, we recall that Δk as well as $\tilde{\kappa}$ is a function of ζ . An optimum spatial variation in ζ could essentially give rise to the possibility of EPs at different physical locations (along z) in a 1D-PC. As an example, we show below that an optimally apodized 1D-PC (1D-APC) which satisfies the adiabatic constraints enables us to observe EPs at discretely separated points along z .

A. Design of an 1D apodized PC and intermodal coupling

We consider a 1D-PC configuration that exhibits varying dielectric filling fraction (ζ) in each unit cell. This variation is essentially dictated through the relation $d_{1M} = d_1 - M\delta$ and $d_{2M} = \Lambda - d_{1M}$. Here, d_{1M} and d_{2M} are the thickness of TiO_2 and SiO_2 layers respectively in M^{th} unit cell ($M = 0, 1, 2, 3, \dots, (N-1)$) for N number of unit cells). The unit cell period, however remains unchanged *i.e.* $\Lambda = d_{1M} + d_{2M} = d_1 + d_2$. This apodization

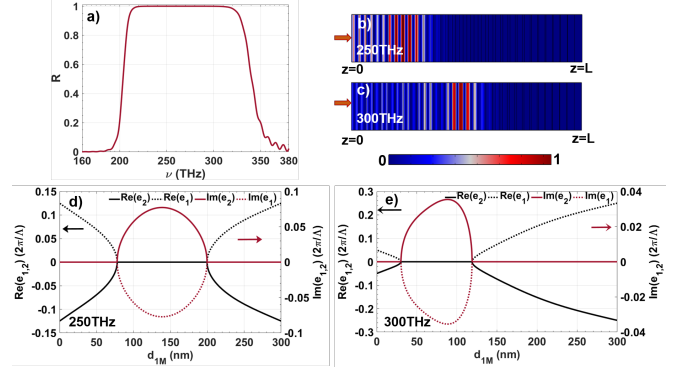


FIG. 2. a) Shows the reflection spectrum for designed 1D-APC. (b) and (c) Shows the mode-field intensities for two different frequencies $\nu_a = 250$ THz and $\nu_b = 300$ THz which are within the PBG of 1D-APC. (d) and (e) Shows the variation in $Re(e_1)$ (dotted black curve), $Im(e_1)$ (dotted maroon curve), $Re(e_2)$ (solid black curve) and $Im(e_2)$ (solid maroon curve) as a function of TiO_2 layer thickness for each unit cell (*i.e.* d_{1M}) at frequencies $\nu_a = 250$ THz and $\nu_b = 300$ THz respectively.

in 1D-PC could be visualized through a longitudinal variation in Δk as well as $\tilde{\kappa}$ by virtue of a monotonic change in average refractive index (\bar{n}) for an *unit cell*. This variation in Δk and $\tilde{\kappa}$ in a 1D-APC geometry leads to an adiabatic evolution of the Stokes vector along the propagation direction and manifests through a broader PBG (≈ 140 THz) in comparison with a conventional (periodic) 1D-PC [30]. This is presented in Fig. 2(a) which shows a broader reflection spectrum for the 1D-APC in comparison with the conventional 1D-PC (Fig.1(a)). In addition, a flat transmission band and the absence of sharp transmission resonances is a distinct feature of 1D-APC. The mode-propagation characteristics for the frequencies within the PBG (of 1D-APC) is explored by drawing a comparison with the mode-field distributions for the equivalent modes within the PBG of a conventional 1D-PC. Figures 2(b) and (c) shows the mode-field distribution for two frequencies $\nu_a = 250$ THz and $\nu_b = 300$ THz which are within the PBG of 1D-APC. In comparison with the mode-field distribution shown in Fig. 1(c), it could be observed that different modes are reflected from spatially separated z values. The smaller frequency ($\nu_a = 250$ THz) is reflected from the regions which are closer to $z = 0$ edge of the 1D-APC in comparison to that for $\nu_b = 300$ THz. This variation is indicative of the fact that the field is localized and exhibits instantaneous localization in different 1D-APC sections. From a different perspective, it is apparent that the variation in dielectric filling fraction (ζ) would result in different eigenvalues (and corresponding eigenvectors) for each unit cell. Accordingly, we plot the eigenvalues e_1 and e_2 as a function of d_{1M} for two frequencies $\nu_a = 250$ THz (Fig. 2(d)) and $\nu_b = 300$ THz (Fig. 2(e)) which are within the PBG of 1D-APC. Each one of the figures shows that the eigen-

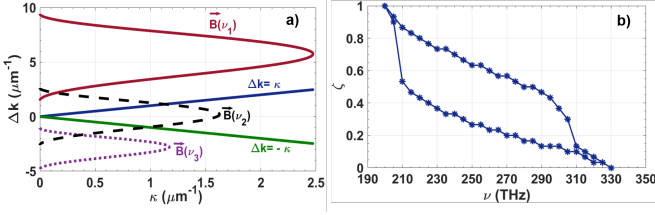


FIG. 3. (a) Shows the variation of \vec{B} in parameter space (spanned by κ and Δk) at different operating frequencies ($\nu_1 = 400$ THz, $\nu_2 = 250$ THz, $\nu_3 = 160$ THz) for the designed 1D-APC. The blue and green solid lines represent the $\Delta k = \kappa$ and $\Delta k = -\kappa$ curves. (b) Shows the location of EPs in different unit cells (with different filling fraction ζ) as a function of frequency (ν).

values (e_1 and e_2) vanish at two different values of d_{1M} *i.e.* at the location of two different unit cells. Therefore, the 1D-APC geometry hosts two EPs for every d_{1M} . Consequently, for a multitude of ζ , there would be multiple EPs in the 1D-APC for a forward-propagating mode to a backscattered mode-coupling process. As discussed before, the regions where $\Re e_1$ and $\Re e_2$ are non-zero in Figs. 2(d) and 2(e) exhibit a \mathcal{PT} -symmetric coupling dynamics between the forward-propagating and backscattered modes. On the other hand, in the regions where e_1 and e_2 are purely imaginary, the mode-coupling process exhibits \mathcal{PT} -symmetry broken manifolds. The illustrations presented in Figs. 2(d) and 2(e) show that for each frequency within the PBG, the 1D-APC hosts two EPs at two different d_{1M} . This essentially implies that there exists one or more than one EPs hosted by each unit cell of the 1D-APC. Therefore, an 1D-APC is expected to host multiple EPs which are spectrally as well as spatially separated from each other. In order to ascertain the spectral location of EPs in the 1D-APC, we plot the evolution of \vec{B} in the parameter space for three different frequencies $\nu_1 = 400$ THz, $\nu_2 = 250$ THz, and $\nu_3 = 160$ THz as shown in Fig.3(a). It could be noted that ν_1 and ν_3 are situated outside PBG of 1D-APC (see Fig. 2(a)). Since, the EPs are depicted by the condition $\Delta k = |\kappa|$, Fig.3(a) also contains the curve $\Delta k = \pm\kappa$ (solid blue and green curves). It is apparent that $\Delta k = \pm\kappa$ curve intersects \vec{B}_{ν_2} at two points and it does not intersect the \vec{B}_{ν_1} curve as well as the \vec{B}_{ν_3} curve in the parameter space. For frequencies close to the band-edge of 1D-APC (say 200 THz or 350 THz), it could be ascertained that there exists only one EP in the eigenvalue spectrum. This is primarily due to the adiabatic constraints followed by the 1D-APC design. In other words, for the band-edge frequencies, the forward and backward propagating modes are decoupled ($\tilde{\kappa}$) at entry ($z = 0$) and exit ($z = L$) face of the crystal. Additionally, $d_{1M} = \Lambda$ for $m = 0$ (or $d_{2M} = \Lambda$ for $m = N$) in case of band-edge frequencies that leads to $\Delta k = 0$ for $\zeta = 0$ (or $\zeta = 1$). Therefore, $\tilde{\kappa} = \Delta k = 0$ depicts the only EP for the band-edge frequencies.

In order to elucidate the aforementioned point, we present the spectral location of EPs as a function of dielectric filling fraction (ζ) or propagation direction (z) in Fig. 3(b). It could be observed that there exists two (2) EPs (at different ζ or z) for all the frequencies well within the PBG of 1D-APC. However, for the band-edge frequencies ($\nu_l = 200$ THz and $\nu_h = 330$ THz), the 1D-APC hosts one EP only. Nevertheless, the area enclosed by the EPs in Fig. 3(b) represents the region of \mathcal{PT} -symmetry broken phase for the 1D-APC. It is interesting to note that the separation between the two EPs for frequencies closer to the band-edges (say $\nu \leq 210$ THz or $\nu \geq 310$ THz) very less and they tend to overlap at the same filling fraction. It is important to note that these EPs are physically positioned *close to* the entry ($z = 0$) and exit ($z = L$) face of the 1D-APC where $\tilde{\kappa}$ is very small. By virtue of this, the PBG corresponding to that unit cell of 1D-APC is relatively smaller in comparison with the PBG for a unit cell close to the center ($z \approx \frac{L}{2}$) of 1D-APC. Due to the fact that the EPs exist at the band-edges of PBG for each unit cell of APC, a smaller PBG would essentially imply closely spaced EPs near the band-edges (see Fig. 3(b)).

B. Geometric phase estimation of reflection band

It is well known that the geometric phase of a pass-band (or transmission band) for a one-dimensional conventional photonic crystal is quantized (0 or π) and it is known as the ‘Zak’ phase. However, the geometric interpretation of backscattered (or reflection) phase from a 1D-PC remains irrelevant. However, in case of 1D-APC, the reflection of different spectral components (within the PBG) takes place from different unit cells (or z) along the propagation direction [30]. For example, the adiabatic following constraint leads to conversion of optical power from the forward-propagating to the backscattered mode predominantly towards the exit face of 1D-APC for frequency $\nu = 250$ THz which could be seen in Fig. 4(a). Through a similar route, it could be shown that different spectral components within the PBG are reflected strongly from different unit cells of 1D-APC [30]. The primary underlying reason could be traced to the variation in $\tilde{\kappa}$ and Δk for each spectral component in the PBG which are non-identical. Consequently, the estimation of geometric phase acquired by different backscattered modes is expected to be different and must play a crucial role in establishing the *bulk-boundary* correspondence in case of 1D-APC. In order to obtain the geometric phase γ , we consider a triad defining the state vector $\vec{S} \equiv [u, v, w]$ where $u = \tilde{A}_i \tilde{A}_r^* + \tilde{A}_r \tilde{A}_i^*$, $v = -i[\tilde{A}_i \tilde{A}_r^* - \tilde{A}_r \tilde{A}_i^*]$ and $w = |\tilde{A}_r|^2 - |\tilde{A}_i|^2$ [30]. The z -component of the state-vector (w) represents the conversion efficiency of optical power from a forward-propagating to a backscattered mode [30]. It is also worth

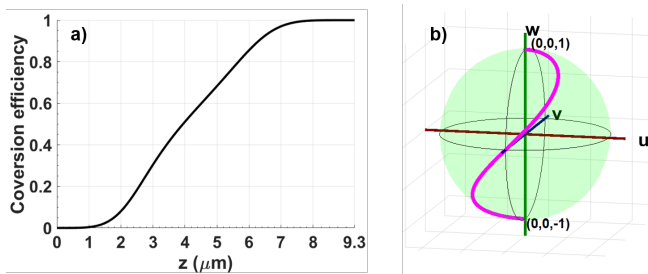


FIG. 4. a) Shows the variation in conversion efficiency ($\frac{w+1}{2}$) for optical power transfer between a forward-propagating mode to a backscattered mode as a function of 1D-APC length (z) for a frequency $\nu_2 = 250 \text{ THz}$ which is within the PBG. (b) Presents the state-vector ($\vec{S} = [u, v, w]$) trajectory on the Bloch sphere for $\nu_2 = 250 \text{ THz}$.

noting that the trajectory of state-vector (\vec{S}) corresponding to the frequencies within the PBG is non-closed. Alternatively, the geometric phase is not a conserved quantity during the dynamical evolution of states owing to the \mathcal{PT} -symmetry broken phase. In general, the solid angle subtended by the state-vector trajectory at the center of the Bloch sphere is used for computing the geometric phase. However, in case of an adiabatic evolution, the state-vector trajectory could be very complicated. In Fig. 4(b), we have plotted such a state-vector trajectory (on the Bloch sphere) corresponding to a frequency $\nu = 250 \text{ THz}$ (which is within the PBG of 1D-APC). It is important to note that $\vec{S} = [0, 0, -1]$ and $\vec{S} = [0, 0, 1]$ represent states in which all the optical power ($\propto |\hat{A}_{f,b}|^2$) is present in the forward-propagating and backscattered mode respectively. Although, the adiabatic evolution of state-vector results in complete optical power transfer from the forward to backward-propagating mode *i.e.* $w = -1$ to $w = 1$, the estimation of acquired geometric phase is quite complicated owing to the spiralling trajectory of \vec{S} on the Bloch-sphere. However, it is interesting to note that \vec{S} goes from $[0, 0, -1]$ to $[0, 0, 1]$ for all the frequencies within the PBG of 1D-APC by virtue of satisfying the adiabatic following constraints. The most important point is to note that the conversion efficiency (or reflectivity) is ‘unity’ for all the frequencies within the PBG of 1D-APC [30]. In other words, \vec{B} goes from $[0, 0, -\Delta k]$ to $[0, 0, \Delta k]$ in the parameter space for all the PBG frequencies (through any trajectory) when the adiabatic following constraints are satisfied [30].

By virtue of the fact that the state-vector \vec{S} adiabatically follows \vec{B} (as per the Bloch equation), the initial and the final value of \vec{B} could also yield the geometric phase (γ). It is known that γ is estimated from angle ϕ (subtended by \vec{B} at the origin $\Delta k = \tilde{\kappa} = 0$) through the relation $\gamma = \frac{\phi}{2}$. In that case, the geometric phase for each spectral component within the PBG is $\frac{\pi}{2}$. In order to elucidate this point, we plot \vec{B} at different z of 1D-APC in the parameter space for $\nu = 250 \text{ THz}$ as

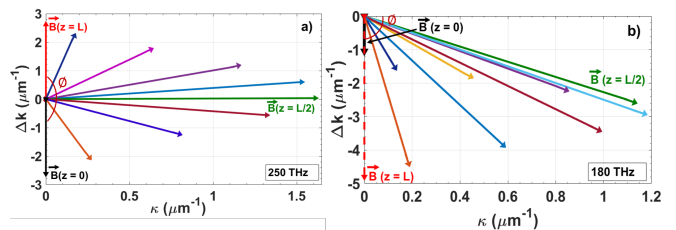


FIG. 5. Represents the evolution of \vec{B} as a function of length (L) of 1D-APC in parameter ($\Delta k - \kappa$) space for a) $\nu_2 = 250 \text{ THz}$ and b) $\nu_4 = 180 \text{ THz}$. ϕ represents the angle subtended by curve \vec{B} at the origin.

shown in Fig. 5(a). At the entry face of 1D-APC ($z = 0$), $\vec{B}(z = 0) = [0, 0, -2.7 \mu\text{m}^{-1}]$ (black arrow) and gradually goes to $\vec{B}(z = L) = [0, 0, +2.7 \mu\text{m}^{-1}]$ (red arrow) at $z = L$. At $z = \frac{L}{2}$, $\Delta k = 0$ and $\tilde{\kappa}$ is maximum (green arrow in Fig. 5(a)) The evolution of \vec{B} in Fig. 5(a) yields $\phi = \pi$ and consequently, $\gamma = \frac{\pi}{2}$. In a similar manner, γ for all the frequencies within the PBG would be $\frac{\pi}{2}$ by virtue of adhering to the constraints imposed by adiabatic following. Hence, it could be asserted that a geometric phase of $\frac{\pi}{2}$ is acquired by a reflected beam in a 1D-APC for the values of parameters which results in \mathcal{PT} -symmetry broken phase. On the contrary, the variation in \vec{B} is plotted as a function of z for $\nu = 180 \text{ THz}$ which is outside the PBG of 1D-APC (see Fig. 5(b)). $\vec{B}(z = 0)$ (black arrow) and $\vec{B}(z = L)$ (red dashed arrow) are both negative as well as co-parallel in this case. Consequently, the geometric phase $\gamma = \frac{\phi}{2} = 0$ for $\nu = 180 \text{ THz}$. In addition, it is apparent that $\Delta k \neq 0$ at any point (or any z) in the 1D-APC.

C. Tamm-plasmon excitations in 1D-APC and topological connection

The presence of a plasmon-active layer adjacent to the all-dielectric 1D-APC results in excitation of multiple Tamm-plasmon modes which are non-degenerate. As an example, we consider a thin ($d_{Au} = 30 \text{ nm}$) layer of gold placed in contact with high index layer (TiO_2) of 1D-APC (see Fig.6(a)). The simulated reflection spectrum (using transfer matrix method) exhibits a sharp resonance within the PBG as shown in Fig.6(b). These resonances are essentially due to Tamm-plasmon mode excitations which are highly localized electromagnetic states. Figure 6(b) depicts the existence of 10 Tamm-plasmon modes within the PBG of 1D-APC. Although there are a few sharp resonances outside the PBG, their mode-field signatures do not resemble that for a Tamm-plasmon mode [32]. In general, the existence of Tamm-plasmon modes is governed by the condition $\phi_{APC} + \phi_{Au} = 2s\pi$ where $s = 0, 1, 2, 3, \dots$ is an integer [33–35]. Here, ϕ_{APC} is the total phase acquired by the reflected beam from the 1D-APC (light incident from Au side), and ϕ_{Au}

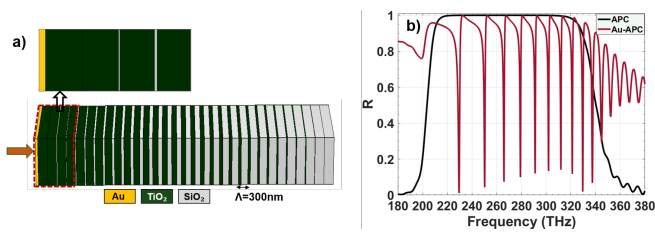


FIG. 6. a) Shows the schematic of the Au -1D-APC heterostructure. The Au -layer is placed adjacent to the high-index TiO_2 layer. The thick brown arrow depicts the direction of light incidence on the Au -1D-APC b) Shows the simulated reflection spectrum of 1D-APC without Au (black solid curve) and that of Au -1D-APC (maroon solid curve).

is the phase acquired by reflected beam at the $Au-TiO_2$ interface. It is worthwhile to reiterate that the dielectric layer (of 1D-APC) adjacent to the Au -film is TiO_2 which is the high index layer. In the present context $\phi_{APC} = \gamma + \alpha$, where α is the dynamic phase acquired by the reflected beam [30]. This could be estimated by noting the fact that the EPs (for a given frequency) are situated in different unit cells (or ζ) of the 1D-APC. For a frequency ν , if the nearest EP (with respect to $z = 0$) is present in the p^{th} -unit cell of 1D-APC, then α could be determined using

$$\alpha = \frac{2\pi\nu}{c} \sum_{M=0}^p [n_1 d_{1M} + n_2 d_{2M}] \quad (5)$$

The knowledge of location for EPs in the 1D-APC (obtained from the eigenvalue spectrum of \hat{H}) would accurately yield the dynamic phase (α) for any frequency of operation (ν). In conjunction with the estimate of γ , this information would allow us to determine the Tamm-plasmon mode resonance frequencies (ν_r). This recipe

provides a flexibility in terms of designing an 1D-APC which would facilitate excitation of Tamm-plasmon mode at a target (desirable) frequency (or wavelength) of operation. One such application could be the generation of higher harmonics or frequency downconversion using optical surface states [36]. In this case, the 1D-APC could be designed such that the Tamm-plasmon modes (localized modes) have resonance frequencies that are governed by the energy conservation and phase-matching constraints imposed by the frequency conversion process.

III. CONCLUSIONS

In conclusion, we presented an all-dielectric 1D-APC design which hosts multiple exceptional points in its eigenvalue spectrum by virtue of exhibiting a non-Hermitian dynamics for a mode-coupling process between a forward-propagating mode to its backscattered counterpart. Although, the 1D-APC does not include any dissipative component, the intermodal coupling mechanism could be classified in terms of \mathcal{PT} -symmetric and \mathcal{PT} -broken phases which are connected through a quantum phase-transition. We also showed that the reflected beam (within the PBG) acquires a geometric phase of $\frac{\pi}{2}$ in the \mathcal{PT} -symmetry broken phase. As a consequence of this outcome, the 1D-APC could be designed for exciting the optical Tamm-plasmon modes at any desirable frequency within the PBG. This design flexibility allows us to employ such architectures for quite a few applications such as efficiently carrying out optical frequency conversion using surface states [36].

IV. DISCLOSURES

The authors declare that there are no conflicts of interest related to this article.

-
- [1] M. Berry, Physics of nonhermitian degeneracies, Czechoslovak Journal of Physics **54**, 1039 (2004).
 [2] W. D. Heiss, The physics of exceptional points, Journal of Physics A: Mathematical and Theoretical **45**, 444016 (2012).
 [3] X.-F. Zhu, Y.-G. Peng, and D.-G. Zhao, Anisotropic reflection oscillation in periodic multilayer structures of parity-time symmetry, Opt. Express **22**, 18401 (2014).
 [4] Z. Lin, H. Ramezani, T. Eichelkraut, T. Kottos, H. Cao, and D. N. Christodoulides, Unidirectional invisibility induced by \mathcal{PT} -symmetric periodic structures, Phys. Rev. Lett. **106**, 213901 (2011).
 [5] W. Wan, Y. Chong, L. Ge, H. Noh, A. Stone, and H. Cao, Time-reversed lasing and interferometric control of absorption, Science (New York, N.Y.) **331**, 889 (2011).
 [6] Y. D. Chong, L. Ge, H. Cao, and A. D. Stone, Coherent perfect absorbers: Time-reversed lasers, Phys. Rev. Lett. **105**, 053901 (2010).
 [7] S. Longhi, \mathcal{PT} -symmetric laser absorber, Phys. Rev. A **82**, 031801 (2010).
 [8] Y. D. Chong, L. Ge, and A. D. Stone, \mathcal{PT} -symmetry breaking and laser-absorber modes in optical scattering systems, Phys. Rev. Lett. **106**, 093902 (2011).
 [9] Y. Sun, W. Tan, H.-q. Li, J. Li, and H. Chen, Experimental demonstration of a coherent perfect absorber with pt phase transition, Phys. Rev. Lett. **112**, 143903 (2014).
 [10] R. Fleury, D. L. Sounas, and A. Alù, Negative refraction and planar focusing based on parity-time symmetric metasurfaces, Phys. Rev. Lett. **113**, 023903 (2014).
 [11] J. Wiersig, Sensors operating at exceptional points: General theory, Phys. Rev. A **93**, 033809 (2016).
 [12] W. Chen, S. Ozdemir, G. Zhao, J. Wiersig, and L. Yang, Exceptional points enhance sensing in an optical microcavity, Nature **548**, 192 (2017).

- [13] J. Wiersig, Enhancing the sensitivity of frequency and energy splitting detection by using exceptional points: Application to microcavity sensors for single-particle detection, *Phys. Rev. Lett.* **112**, 203901 (2014).
- [14] H. Xu, D. Mason, L. Jiang, and J. Harris, Topological energy transfer in an optomechanical system with exceptional points, *Nature* **537** (2016).
- [15] L. Ge, Y. D. Chong, and A. D. Stone, Conservation relations and anisotropic transmission resonances in one-dimensional \mathcal{PT} -symmetric photonic crystal heterostructures, *Phys. Rev. A* **85**, 023802 (2012).
- [16] J. Doppler, A. Mailybaev, J. Böhm, U. Kuhl, A. Girschik, F. Libisch, T. Milburn, P. Rabl, N. Moiseyev, and S. Rotter, Dynamically encircling exceptional points in a waveguide: asymmetric mode switching from the breakdown of adiabaticity, *Nature* **537** (2016).
- [17] Y. Ota, R. Katsumi, K. Watanabe, S. Iwamoto, and Y. Arakawa, Topological photonic crystal nanocavity laser, *Communications Physics* **1** (2018).
- [18] L. Ge and A. D. Stone, Parity-time symmetry breaking beyond one dimension: The role of degeneracy, *Phys. Rev. X* **4**, 031011 (2014).
- [19] X. Zhu, H. Ramezani, C. Shi, J. Zhu, and X. Zhang, \mathcal{PT} -symmetric acoustics, *Phys. Rev. X* **4**, 031042 (2014).
- [20] K. Ding, Z. Q. Zhang, and C. T. Chan, Coalescence of exceptional points and phase diagrams for one-dimensional \mathcal{PT} -symmetric photonic crystals, *Phys. Rev. B* **92**, 235310 (2015).
- [21] T. Goldzak, A. A. Mailybaev, and N. Moiseyev, Light stops at exceptional points, *Phys. Rev. Lett.* **120**, 013901 (2018).
- [22] J.-R. Li, L.-L. Zhang, W.-B. Cui, and W.-J. Gong, Topological properties in non-hermitian tetratomic schrieffer-heeger lattices, *Phys. Rev. Research* **4**, 023009 (2022).
- [23] F. Mostafavi, C. Yuce, O. S. Magaña Loaiza, H. Schomeerus, and H. Ramezani, Robust localized zero-energy modes from locally embedded \mathcal{PT} -symmetric defects, *Phys. Rev. Research* **2**, 032057 (2020).
- [24] A. Guo, G. J. Salamo, D. Duchesne, R. Morandotti, M. Volatier-Ravat, V. Aimez, G. A. Siviloglou, and D. N. Christodoulides, Observation of \mathcal{PT} -symmetry breaking in complex optical potentials, *Phys. Rev. Lett.* **103**, 093902 (2009).
- [25] B. Peng, S. Özdemir, S. Rotter, H. Yilmaz, M. Liertzer, F. Monifi, C. Bender, F. Nori, and L. Yang, Loss-induced suppression and revival of lasing, *Science* (New York, N.Y.) **346**, 328–332 (2014).
- [26] C. Dembowski, H.-D. Gräf, H. L. Harney, A. Heine, W. D. Heiss, H. Rehfeld, and A. Richter, Experimental observation of the topological structure of exceptional points, *Phys. Rev. Lett.* **86**, 787 (2001).
- [27] S.-Y. Lee, J.-W. Ryu, S. W. Kim, and Y. Chung, Geometric phase around multiple exceptional points, *Phys. Rev. A* **85**, 064103 (2012).
- [28] N. Flemens and J. Moses, Hermitian nonlinear wave mixing controlled by a pt -symmetric phase transition, *Phys. Rev. Lett.* **129**, 153901 (2022).
- [29] A. Yariv and P. Yeh, *Optical Waves in Crystals Propagation and Control of Laser Radiation* (New York Wiley, 1984).
- [30] S. Sharma, A. Mondal, and R. Das, Geometric representation of adiabatic distributed-bragg-reflectors and broadening the photonic bandgap, *Opt. Express* **29**, 43303 (2021).
- [31] A. Laha, D. Beniwal, S. Dey, A. Biswas, and S. Ghosh, Third-order exceptional point and successive switching among three states in an optical microcavity, *Phys. Rev. A* **101**, 063829 (2020).
- [32] S. Sharma, A. Mondal, and R. Das, Infrared rainbow trapping via optical tamm modes in an one-dimensional dielectric chirped photonic crystals, *Opt. Lett.* **46**, 4566 (2021).
- [33] M. K. Shukla and R. Das, Tamm-plasmon polaritons in one-dimensional photonic quasi-crystals, *Opt. Lett.* **43**, 362 (2018).
- [34] M. Xiao, Z. Q. Zhang, and C. T. Chan, Surface impedance and bulk band geometric phases in one-dimensional systems, *Phys. Rev. X* **4**, 021017 (2014).
- [35] A. P. Vinogradov, A. V. Dorofeenko, S. G. Erokhin, M. Inoue, A. A. Lisiansky, A. M. Merzlikin, and A. B. Granovsky, Surface state peculiarities in one-dimensional photonic crystal interfaces, *Phys. Rev. B* **74**, 045128 (2006).
- [36] B. I. Afinogenov, A. A. Popkova, V. O. Bessonov, B. Lukyanchuk, and A. A. Fedyanin, Phase matching with tamm plasmons for enhanced second- and third-harmonic generation, *Phys. Rev. B* **97**, 115438 (2018).